

Supporting information for

CO Oxidation Promoted by Gold Atoms Loosely Attached in AuFeO_3^- Cluster Anions

Zhen Yuan,^{†,‡} Xiao-Na Li,^{†} and Sheng-Gui He^{*†}*

[†]Beijing National Laboratory for Molecular Sciences, State Key Laboratory for Structural Chemistry of Unstable and Stable Species, Institute of Chemistry, Chinese Academy of Sciences, Beijing 100190, P. R. China.

[‡]University of Chinese Academy of Sciences, Beijing 100049, P. R. China.

*Corresponding author, E-mail: lxn@iccas.ac.cn; shengguihe@iccas.ac.cn;

Phone: +86-10-62536990; Fax: +86-10-62559373

Contents

1. Experimental methods
2. Theoretical methods
3. Additional experimental results (Figure S1)
4. Additional theoretical results (Figures S2–S10)

1. Experimental methods

The details of the experimental setup can be found in previous studies (unpublished results),¹⁻³ and only a brief outline of the experiments is given below. The heteronuclear $\text{AuFe}_x\text{O}_y^-$ and pure Fe_xO_y^- oxide cluster anions are generated by laser ablation of an Au/Fe mixed metal disk (1:1 Au:Fe molar ratio) in the presence of O_2 (1%) seeded in a He carrier gas (7 atm). The AuFeO_3^- and $\text{AuFe}_2\text{O}_4^-$ oxide cluster anions are mass-selected using a quadrupole mass filter and then entered into an ion trap reactor or a hexapole collision cell to react with reactant molecules. Note that slightly before the cluster ions entering into the ion trap, a pulse of helium gas is delivered into the trap so that the clusters can be cooled and confined in the ion trap. After confining the cluster ions in the ion trap for about 0.7 ms, the reactant gas molecules (10% CO/N_2 or N_2) are delivered to interact with the clusters for a period of time (≈ 2.3 ms) (unpublished results). The mass-selected FeO_3^- and Fe_2O_4^- cluster anions are confined and reacted with pure CO in the ion trap for about 52.3 and 2.3 ms, respectively. In the collision cell experiment, the mass-selected AuFeO_3^- and $\text{AuFe}_2\text{O}_4^-$ clusters enter into a 50 mm long hexapole collision cell and interact with pure CO or N_2 directly for about 19 μs . Before the prepared gases (CO, N_2 , CO/N_2 , and O_2/He) are pulsed into the vacuum system, it is useful to pass them through copper tube coils at low temperature (~ 200 K, dry ice in ethanol) in order to remove a trace amount of water from the gas handling system. The intracluster vibrations in the ion trap are likely equilibrated to room-temperature before reacting with CO. The reactant and

product ions exiting from the reactor are detected by a reflection time-of-flight mass spectrometer (TOF-MS).³

- (1) Yuan, Z.; Zhao, Y.-X.; Li, X.-N.; He, S.-G. Reactions of $V_4O_{10}^+$ Cluster Ions with Simple Inorganic and Organic Molecules. *Int. J. Mass Spectrom.* **2013**, *354–355*, 105-112.
- (2) Wu, X.-N.; Ma, J.-B.; Xu, B.; Zhao, Y.-X.; Ding, X.-L.; He, S.-G. Collision-Induced Dissociation and Density Functional Theory Studies of CO Adsorption over Zirconium Oxide Cluster Ions: Oxidative and Nonoxidative Adsorption. *J. Phys. Chem. A* **2011**, *115*, 5238-5246.
- (3) Wu, X.-N.; Xu, B.; Meng, J.-H.; He, S.-G. C-H Bond Activation by Nanosized Scandium Oxide Clusters in Gas-Phase. *Int. J. Mass Spectrom.* **2012**, *310*, 57-64.

2. Theoretical methods

Density functional theory (DFT) calculations with the hybrid B3LYP^{1,2} functional and the Gaussian 09³ program are performed to study the reaction mechanisms of AuFeO_3^- oxide cluster anions with CO. The AuFeO_3^- cluster is optimized by employing SDD basis sets⁴ for Au and 6-311+g* basis sets^{5,6} for other atoms. This level of calculation has been tested to give reasonably good results for the mechanism study of FeO_{1-3} and $\text{FeO}_{4,5}$ clusters with CO.⁷ Test calculations for AuFeO_3^- with employing LANL2DZ⁸ basis sets for gold and 6-311+g* basis sets for other atoms (Figure S10) give very similar ground state structure of AuFeO_3^- as that using SDD. In the reaction mechanism calculations, the relaxed potential energy surface scan is used extensively to obtain good guess structures for the intermediates and the transition states (TS) along the reaction pathways. The TSs are optimized by using the Berny algorithm method.⁹ Intrinsic reaction coordinate calculations^{10,11} are also performed so that each TS connects two appropriate local minima. Vibrational frequency calculations are carried out to check that reaction intermediates and TSs have zero and only one imaginary frequency, respectively. The meta-generalized gradient approximation functionals (such as TPSS) have been suggested necessary for systems containing gold.¹²⁻¹⁵ Thus, the most stable isomers of $\text{AuFeO}_{2,3}^-$ and the reaction mechanism of $\text{AuFeO}_3^- + \text{CO}$ are re-calculated using TPSS functional.¹⁶ It turns out that both TPSS and B3LYP functionals predict similar ground state structures for AuFeO_3^- . However, the TPSS functional predicts the binding energy of the neutral gold atom in AuFeO_3^- is 1.355 eV, which is not in the range of experimental estimated center-of-

mass collisional energy ($0.14 < E_c < 0.9$ eV). The Basis set superposition error (BSSE) is calculated for the binding energies of a few CO-AuFeO₃⁻ complexes employing the counterpoise method.¹⁷ The results indicate that the BSSE is negligible. The zero-point vibration corrected energies and the Gibbs free energies at 298 K ($\Delta H_{0K}/\Delta G_{298K}$) are reported.

- (1) Lee, C.; Yang, W.; Parr, R. G. Development of the Colle-Salvetti Correlation-Energy Formula into a Functional of the Electron Density. *Phys. Rev. B* **1988**, *37*, 785-789.
- (2) Becke, A. D. Density-Functional Thermochemistry. III. The Role of Exact Exchange. *J. Chem. Phys.* **1993**, *98*, 5648-5652.
- (3) Frisch, M. J.; Trucks, G. W.; Schlegel, H. B.; Scuseria, G. E.; Robb, M. A.; Cheeseman, J. R.; Scalmani, G.; Barone, V.; Mennucci, B.; Petersson, G. A.; Nakatsuji, H.; Caricato, M.; Li, X.; Hratchian, H. P.; Izmaylov, A. F.; Bloino, J.; Zheng, G.; Sonnenberg, J. L.; Hada, M.; Ehara, M.; Toyota, K.; Fukuda, R.; Hasegawa, J.; Ishida, M.; Nakajima, T.; Honda, Y.; Kitao, O.; Nakai, H.; Vreven, T.; Montgomery, J. A., Jr.; Peralta, J. E.; Ogliaro, F.; Bearpark, M.; Heyd, J. J.; Brothers, E.; Kudin, K. N.; Staroverov, V. N.; Kobayashi, R.; Normand, J.; Raghavachari, K.; Rendell, A.; Burant, J. C.; Iyengar, S. S.; Tomasi, J.; Cossi, M.; Rega, N.; Millam, J. M.; Klene, M.; Knox, J. E.; Cross, J. B.; Bakken, V.; Adamo, C.; Jaramillo, J.; Gomperts, R.; Stratmann, R. E.; Yazyev, O.; Austin, A. J.; Cammi, R.; Pomelli, C.; Ochterski, J. W.; Martin, R. L.; Morokuma, K.; Zakrzewski, V. G.; Voth, G. A.; Salvador, P.; Dannenberg, J. J.; Dapprich, S.; Daniels, A. D.; Farkas, O.; Foresman, J. B.; Ortiz, J. V.; Cioslowski, J.; Fox, D. J.; Gaussian 09, Revision A.1, Gaussian, Inc., Wallingford CT, 2009.
- (4) Andrae, D.; Häußermann, U.; Dolg, M.; Stoll, H.; Preuß, H. Energy-Adjusted ab initio Pseudopotentials for the Second and Third Row Transition Elements. *Theor. Chim. Acta.* **1990**, *77*, 123-141.
- (5) Hehre, W. J.; Ditchfield, R.; Pople, J. A. Self-Consistent Molecular Orbital Methods. XII. Further Extensions of Gaussian-Type Basis Sets for Use in Molecular Orbital Studies of Organic Molecules. *J. Chem. Phys.* **1972**, *56*, 2257-2261.
- (6) Krishnan, R.; Binkley, J. S.; Seeger, R.; Pople, J. A. Self-Consistent Molecular Orbital Methods. XX. A Basis Set for Correlated Wave Functions. *J. Chem. Phys.* **1980**, *72*, 650-654
- (7) Xue, W.; Wang, Z.-C.; He, S.-G.; Xie, Y.; Bernstein, E. R. Experimental and Theoretical Study of the Reactions Between Small Neutral Iron Oxide Clusters and Carbon Monoxide. *J. Am. Chem. Soc.* **2008**, *130*, 15879-15888.
- (8) Dupuis, M.; Rys, J.; King, H. F. Evaluation of Molecular Integrals over Gaussian Basis Functions. *J. Chem. Phys.* **1976**, *65*, 111-116.
- (9) Schlegel, H. B. Optimization of Equilibrium Geometries and Transition Structures. *J. Comput. Chem.* **1982**, *3*, 214-218.
- (10) Gonzalez, C.; Schlegel, H. B. An Improved Algorithm for Reaction Path Following. *J. Chem. Phys.* **1989**, *90*,

2154-2161.

- (11) Gonzalez, C.; Schlegel, H. B. Reaction Path Following in Mass-Weighted Internal Coordinates. *J. Phys. Chem.* **1990**, *94*, 5523-5527.
- (12) Wang, S. G.; Schwarz, W. H. E. Quasi-Relativistic Density Functional Study of Auophilic Interactions. *J. Am. Chem. Soc.* **2004**, *126*, 1266-1276.
- (13) Johansson, M. P.; Lechtken, A.; Schooss, D.; Kappes, M. M.; Furche, F. 2D-3D Transition of Gold Cluster Anions Resolved. *Phys. Rev. A* **2008**, *77*, 053202.
- (14) Aikens, C. M. Effects of Core Distances, Solvent, Ligand, and Level of Theory on the TDDFT Optical Absorption Spectrum of the Thiolate-Protected Au₂₅ Nanoparticle. *J. Phys. Chem. A* **2009**, *113*, 10811-10817.
- (15) Ferrighi L.; Hammer, B.; Madsen, G. K. H. 2D-3D Transition for Cationic and Anionic Gold Clusters: A Kinetic Energy Density Functional Study. *J. Am. Chem. Soc.* **2009**, *131*, 10605-10609.
- (16) Tao, J. M.; Perdew, J.; Staroverov, V. N.; Scuseria, G. E. Climbing the Density Functional Ladder: Nonempirical Meta-Generalized Gradient Approximation Designed for Molecules and Solids. *Phys. Rev. Lett.* **2003**, *91*, 146401.
- (17) van Duijneveldt, F. B.; van Duijneveldt-van de Rijdt, J. G. C. M.; van Lenthe, J. H. State of the Art in Counterpoise Theory. *Chem. Rev.* **1994**, *94*, 1873-1885.

3. Additional experimental results

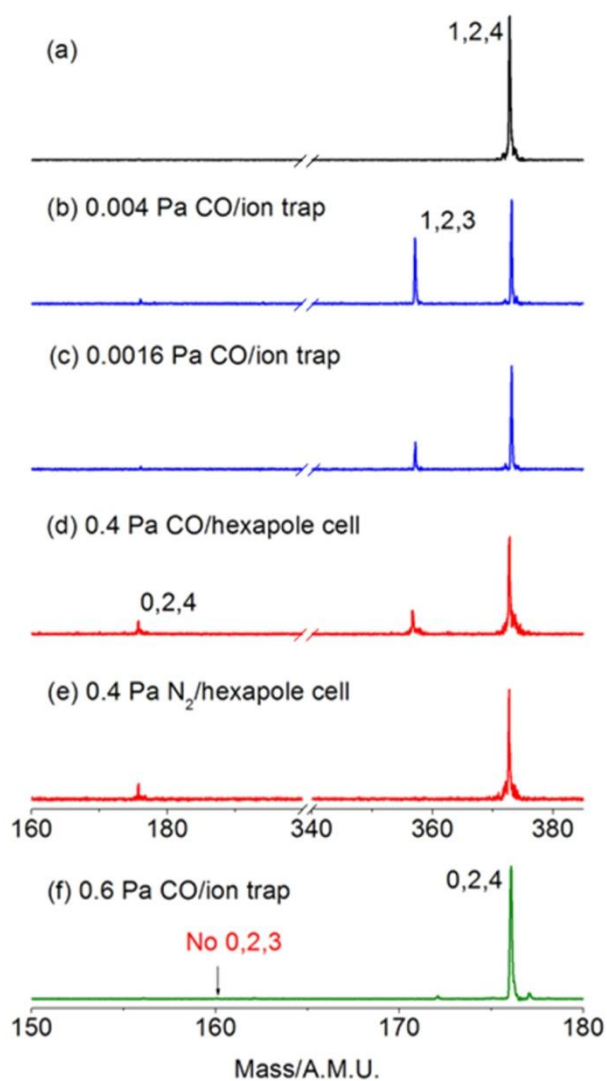


Figure S1. The TOF mass spectra for reactions of mass-selected $\text{AuFe}_2\text{O}_4^-$ (a-e) in an ion trap reactor (b,c/CO) for about 2.3 ms and in a hexapole collision cell (d/CO and e/ N_2) for about 19 μs . The reaction of mass-selected Fe_2O_4^- with CO in an ion trap reactor for about 2.3 ms is given in (f). The maximal reactant gas pressures are given in Pa.

3. Additional theoretical results

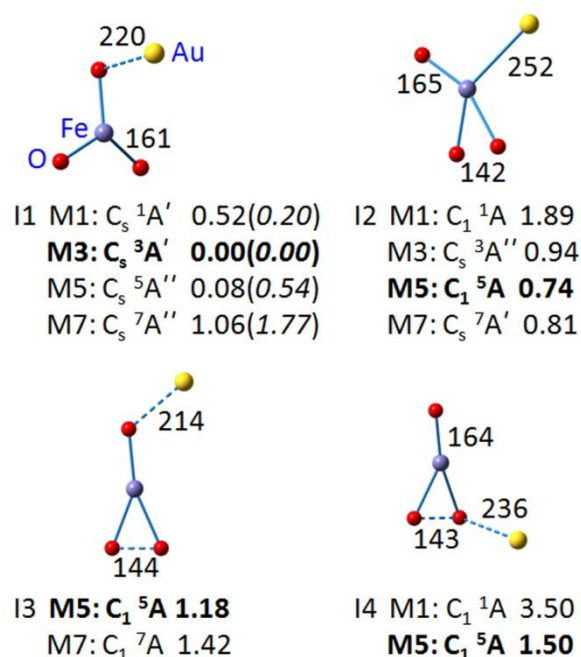


Figure S2. DFT calculated isomers for cluster AuFeO_3^- . The symmetries, electronic states, and the zero-point vibration corrected energies ($\Delta H_{0\text{K}}$ in eV) with respect to the most stable isomer are given below each structure. The *italics* in the parenthesis are the results calculated using TPSS functional. Bond lengths are given in pm. For isomer I2, the gold atoms are negatively charged (M1: -0.290 |e|; M3: -0.143 |e|; M5: -0.417 |e|; M7: -0.547 |e|), and the larger binding energies for spin multiplicities M3 (${}^3\text{AuFeO}_3^- \rightarrow {}^2\text{Au} + {}^4\text{FeO}_3^-$ $\Delta H_{0\text{K}} = 1.228$ eV), M5 (${}^5\text{AuFeO}_3^- \rightarrow {}^2\text{Au} + {}^4\text{FeO}_3^-$ $\Delta H_{0\text{K}} = 1.427$ eV), and M7 (${}^7\text{AuFeO}_3^- \rightarrow {}^2\text{Au} + {}^4\text{FeO}_3^-$ $\Delta H_{0\text{K}} = 1.356$ eV) result from the strong polarization interaction between the gold atom and the iron atom. In these cases, the gold atoms are not loosely attached. The structure of ${}^4\text{FeO}_3^-$ can be found in Figure S7 (I2).

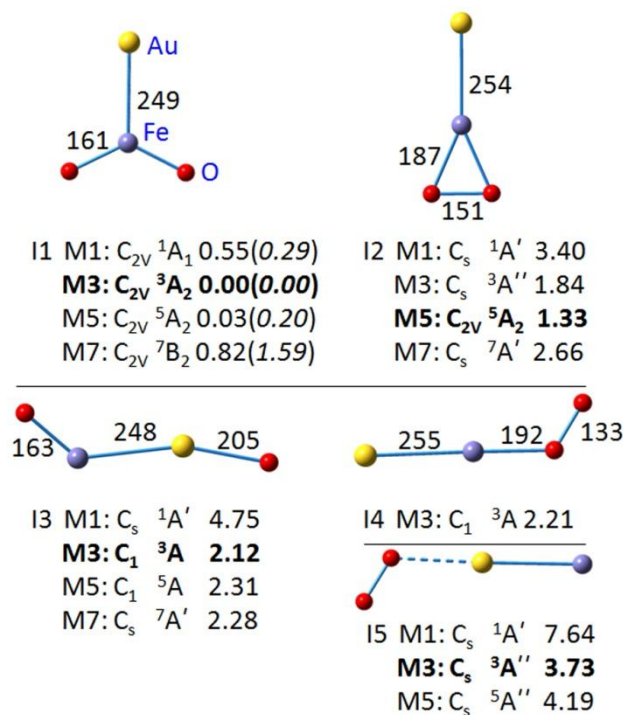


Figure S3. DFT calculated isomers for cluster $AuFeO_2^-$. The symmetries, electronic states, and the zero-point vibration corrected energies (ΔH_{0K} in eV) with respect to the most stable isomer are given below each structure. The *italics* in the parenthesis are the results calculated using TPSS functional. Bond lengths are given in pm.

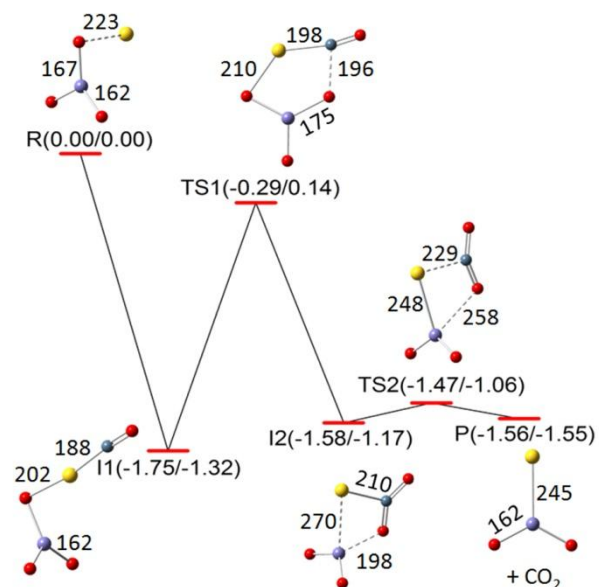


Figure S4. DFT (TPSS) calculated potential-energy profile for reaction $\text{AuFeO}_3^- + \text{CO} \rightarrow \text{AuFeO}_2^- + \text{CO}_2$. The zero-point vibration corrected energies and Gibbs free energies at 298 K ($\Delta H_{0\text{K}}/\Delta G_{298\text{K}}$ in eV) with respect to the separated reactants are given. Bond lengths are given in pm.

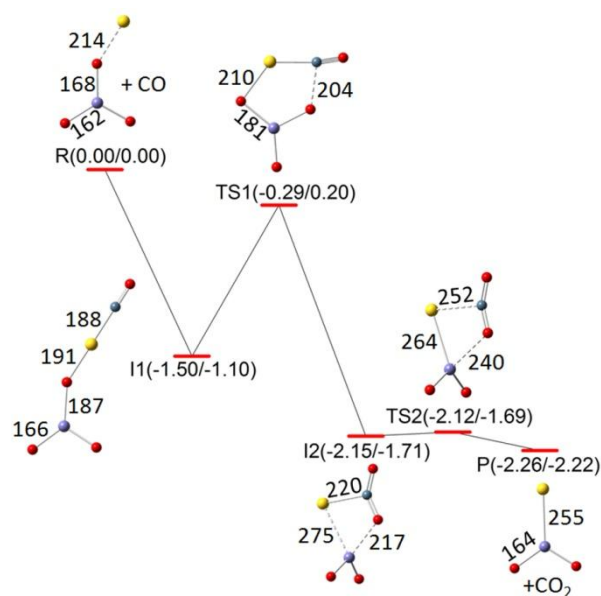


Figure S5. DFT (B3LYP) calculated potential-energy profile for reaction ${}^5\text{AuFeO}_3^- + \text{CO} \rightarrow {}^5\text{AuFeO}_2^- + \text{CO}_2$ at the quintet state. The zero-point vibration corrected energies and Gibbs free energies at 298 K ($\Delta H_{0\text{K}}/\Delta G_{298\text{K}}$ in eV) with respect to the separated reactants are given. Bond lengths are given in pm.

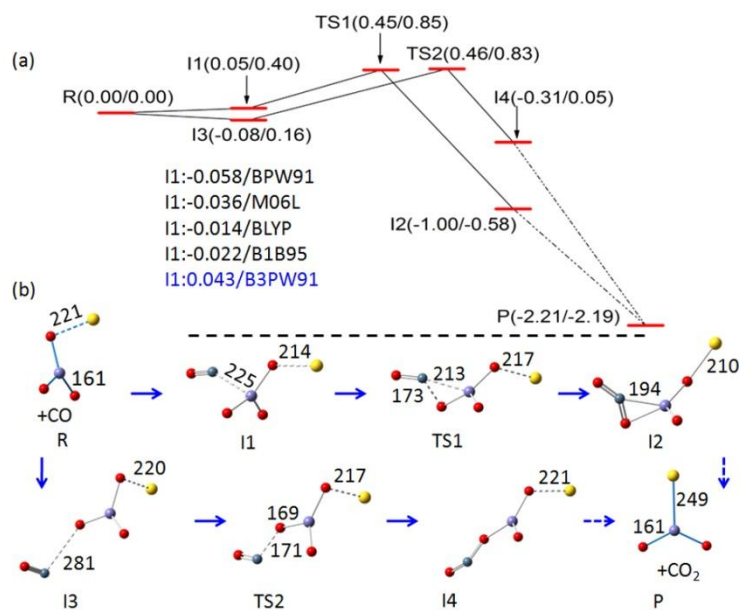


Figure S6. (a) DFT (B3LYP) calculated triplet potential energy profiles for reaction $\text{AuFeO}_3^- + \text{CO} \rightarrow \text{AuFeO}_2^- + \text{CO}_2$ without the direct participation of Au atom at the beginning of the reaction. (b) The structures of the reaction intermediates, transition states, and products. The zero-point vibration corrected energies and Gibbs free energies at 298 K ($\Delta H_{0\text{K}}/\Delta G_{298\text{K}}$ in eV) with respect to the separate reactants are given. Bond lengths are given in pm.

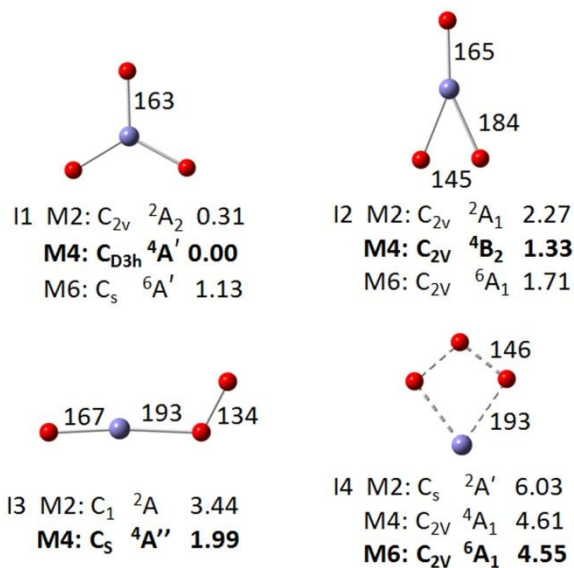


Figure S7. DFT (B3LYP) calculated isomers for clusters FeO_3^- . The symmetries, electronic states, and the zero-point vibration corrected energies (ΔH_{0K} in eV) with respect to the most stable isomer are given below each structure. Bond lengths are given in pm.

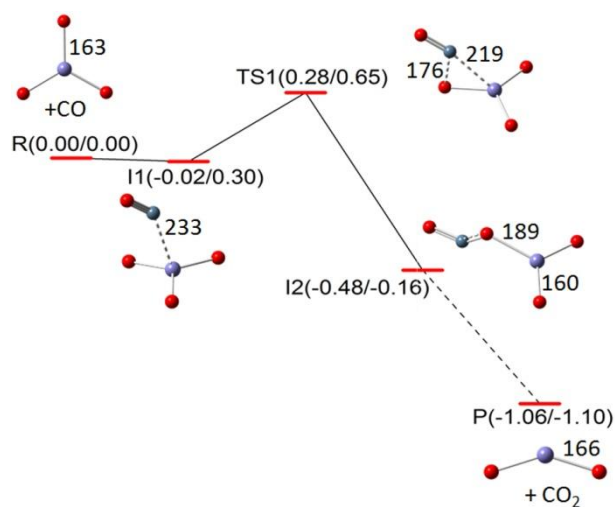


Figure S8. DFT (B3LYP) calculated potential-energy profile for reaction ${}^4\text{FeO}_3^- + \text{CO} \rightarrow {}^4\text{FeO}_2^- + \text{CO}_2$. The zero-point vibration corrected energies and Gibbs free energies at 298 K ($\Delta H_{0\text{K}}/\Delta G_{298\text{K}}$ in eV) with respect to the separated reactants are given. Bond lengths are given in pm.

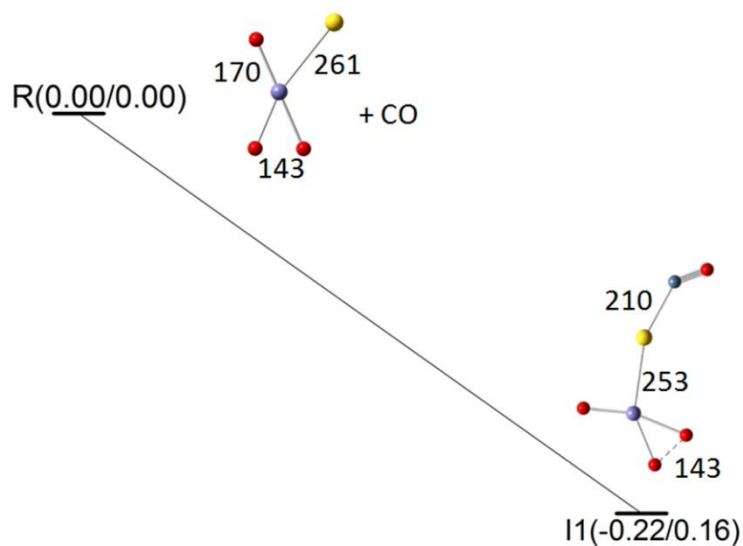


Figure S9. DFT (B3LYP) calculated CO adsorption on isomer I2 at the quintet state (see Figure S2). The zero-point vibration corrected energies and Gibbs free energies at 298 K ($\Delta H_{0K}/\Delta G_{298K}$ in eV) with respect to the separated reactants are given. Bond lengths are given in pm. The CO adsorption energy on I2 is small ($\Delta H_{0K} = 0.22$ eV), so that dissociation into the reactants ($\text{AuFeO}_3^- + \text{CO}$) will be dominant and the reaction efficiency will be low. The gold atom in this case cannot function as the effective trapping site for CO due to its negative charge (-0.417 |e|). Thus, the gold atom bonded with the iron atom does not play the same roles as that bonded with the oxygen atom.

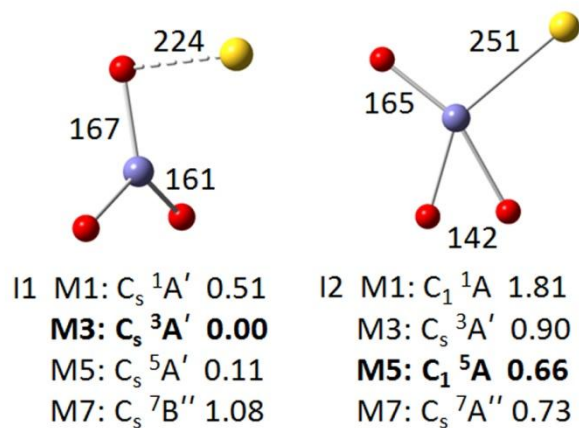


Figure S10. DFT (B3LYP) calculated geometrical structures of low-lying isomers of cluster AuFeO₃⁻ in the case that LANL2DZ and 6-311+g* basis sets are used for Au and other atoms, respectively.

Table S1. The calculated Gibbs free energies (eV) for intermediate (I1) and transition state (TS1) (see details in Figure 2) at different temperatures. The rates of back dissociation k_d (I1 \rightarrow AuFeO₃⁻ + CO) and internal conversion k_{ic} (I1 \rightarrow TS1 \rightarrow I2) are given.

| T / K | $\Delta G/\text{I1}$ | $\Delta G/\text{TS1}$ | k_d (I1 \rightarrow AuFeO ₃ ⁻ + CO) | k_{ic} (I1 \rightarrow TS1 \rightarrow I2) | k_d / k_{ic} |
|----------------|----------------------|-----------------------|---|--|----------------|
| 298 | -1.16 | 0.16 | $23 \times 10^6 \text{ s}^{-1}$ | $8.9 \times 10^6 \text{ s}^{-1}$ | 2.6 |
| 200 | -1.30 | -0.002 | $7.1 \times 10^6 \text{ s}^{-1}$ | $5.2 \times 10^6 \text{ s}^{-1}$ | 1.4 |
| 150 | -1.38 | -0.08 | $4.0 \times 10^6 \text{ s}^{-1}$ | $4.1 \times 10^6 \text{ s}^{-1}$ | 1.0 |
| 100 | -1.45 | -0.16 | $1.7 \times 10^6 \text{ s}^{-1}$ | $2.8 \times 10^6 \text{ s}^{-1}$ | 0.6 |
| 50 | -1.52 | -0.24 | $1.7 \times 10^6 \text{ s}^{-1}$ | $2.9 \times 10^6 \text{ s}^{-1}$ | 0.6 |